R. & M. No. 3367

MINISTRY OF AVIATION

AERONAUTICAL RESEARCH COUNCIL
REPORTS AND MEMORANDA

Streamwise Edge Effects in the Turbulent Boundary Layer on a Flat Plate of Finite Aspect Ratio

By E. B. DAVIES and A. D. YOUNG

DEPARTMENT OF AERONAUTICAL ENGINEERING, QUEEN MARY COLLEGE,
UNIVERSITY OF LONDON

LONDON: HER MAJESTY'S STATIONERY OFFICE
1964
PRICE 12s. 6d. NET

Streamwise Edge Effects in the Turbulent Boundary Layer on a Flat Plate of Finite Aspect Ratio

By E. B. Davies and A. D. Young

Department of Aeronautical Engineering, Queen Mary College, University of London

*Reports and Memoranda No. 3367**
February, 1963

Summary.

A detailed investigation of the turbulent boundary layer on a flat plate of finite aspect ratio at zero incidence has been made, incorporating measurements of mean velocity profiles and skin friction over one surface of the plate. Skin friction was measured using Prof. Preston's surface-tube technique with the N.P.L. calibration, and this is justified by comparison with the measured momentum defect.

These results are compared with others recorded on a 'two-dimensional' plate (i.e. one that spanned the wind tunnel), and the effects of the streamwise edges on the boundary-layer flow on the plate surface are shown to be limited to regions of the plate surface near the edges of the order of a boundary-layer thickness in width.

The drag results are analysed to provide an indication of the effect of the edges on the drag of the plate, but a more general assessment of this effect follows from an analysis of the spanwise distribution of the boundary-layer parameters near the edges of the plate. The recommended relation that results for the ratio of the skin-friction coefficient of a plate of finite aspect ratio (C_F) to that of a corresponding two-dimensional plate (C_{F0}) is:

$$C_F/C_{F0} = 1 + C_{F0}l/b,$$

where l is the length and b is the span of the plate.

This aspect-ratio effect is considerably smaller than that estimated by Hughes (Ref. 2) and, contrary to Hughes' conclusions, is such that the drag results from tests on three-dimensional plates used as a basis for the Schoenherr and Prandtl-Schlichting laws generally require insignificant modification on account of it (never greater than about 4%). These, or similar newer laws can therefore continue to be regarded as reliable guides for most engineering purposes to the skin friction in two dimensions. A re-analysis of Hughes' results brings them into line with the present work.

LIST OF CONTENTS

* Replaces A.R.C. 24 596.

LIST OF CONTENTS—*continued*

---

1. *Introduction.*

In Reference 2, Hughes presented many measurements of the overall drag of submerged sheets and pontoons which were towed in a water tank, and from these he deduced the existence of a very pronounced effect of aspect ratio on the skin-friction drag of flat surfaces. On the basis of his analysis, he concluded that the standard empirical laws which had hitherto been used to describe the skin friction of flat plates under two-dimensional flow conditions (e.g. the Schoenherr or Prandtl-Schlichting laws) predicted values of C_F which were up to 15% too high, and he proposed a new skin-friction formula which purported to correct this error. This new interpretation of the results of drag tests on flat plates was subsequently given some support by Townsend[3] who presented a semi-theoretical analysis of the three-dimensional flow over a flat plate of finite aspect ratio which could explain the effect observed by Hughes if certain disposable constants were suitably chosen. This theory required that the effect of aspect ratio on the boundary layer be spread over the whole span of the plate and not be simply confined to regions on the plate surface in the vicinity of the edges. This was clearly a result of far-reaching importance in the interpretation of tests of flat plates of finite span, for it could no longer be said that even the flow along the centre-line could be two-dimensional in nature.

However, Hughes' new two-dimensional skin friction—Reynolds number relationship and its associated aspect-ratio correction were difficult to reconcile with the existing body of aerodynamic

data and semi-empirical theories for skin friction in flat-plate turbulent boundary layers and Hughes' mode of analysis and interpretation of his results were open to question. Consequently, the matter called for further investigation.

In this paper, further work on the nature of the aspect-ratio effect on the drag of flat plates is described and Hughes' conclusions are reconsidered in the light of these new data. Detailed measurements of the boundary layers over the surfaces of two plates are presented; one plate being of nominal span 6 in., and the other was a 'two-dimensional' plate spanning the tunnel. Velocity traverses were recorded with Pitot tubes, both over the plate surface and outside the edges of the finite-span plate, and skin friction was measured over the plate surface using Prof. Preston's surface-tube technique[4]. This technique was then checked by integrating the values of local skin-friction coefficient C_f so determined to give a chordwise growth in momentum thickness θ which was compared with the growth calculated from the velocity profiles. The N.P.L. calibration[5] for the Preston tube technique was found to give best agreement between the two.

A brief description of the experimental arrangement and test programme is given in Section 2, and in Section 3 the measurements of θ and C_f are presented and the general features of flow over a plate of finite span are discussed. In Section 4 the boundary-layer growth along the centre-line of the finite-span plate is compared with that along the 'two-dimensional' plate and the results are examined to see whether they support the hypothesis that the aspect-ratio effect extends over the span of the plate. The centre-line growth is also compared with various empirical standard laws for two-dimensional boundary-layer development. The spreading of the edge effect on to the plate surface is considered in more detail in Section 5 and the drag data are analysed to assess the magnitude of the aspect-ratio effect on the drag of the test plate. However, to extend the validity of the data they are fitted in Section 7 into a more general picture of the growth of the edge effect along the plate in the streamwise direction after a measure of similarity at different chordwise stations is demonstrated in Section 6. Finally, in Section 8 the data on edge effects obtained from the present work are compared with those of previous experimenters and in particular the work of Hughes is reconsidered.

It is concluded that the effect of aspect ratio on the drag of flat plates of finite span is small and is such that the older established empirical skin-friction 'laws' of, say, Prandtl-Schlichting or Schoenherr based on experiments on such plates may still be used with adequate accuracy for most engineering purposes to describe the two-dimensional variation of skin friction with Reynolds number, and Hughes' proposal of a new law, with its correspondingly large aspect-ratio effect, is rejected.

2. *The Experimental Apparatus and Test Programme.*

The experiments consisted of measurements of velocity profiles and skin friction in the boundary layer on, and around the edges of, flat plates mounted vertically in the 4 ft × 3 ft low-speed, low-turbulence closed-circuit wind tunnel at Queen Mary College. The plates were constructed from $\frac{3}{8}$ in. thick paper Tufnol on to which was stuck a 4 in. length of elliptic leading edge made of varnished hardwood. A trailing edge was also incorporated in the initial stages but difficulty was encountered in aligning it properly with the plate axis so it was removed and all the main tests were performed without it.

The two main plates used in the experiments were a plate cut to span the tunnel (referred to as the two-dimensional plate in what follows) and one of a nominal 6 in. span on to which semi-circular

streamwise edges were formed with the aid of semi-circular brass rod of $\frac{3}{8}$ in. diameter (referred to as the finite-span or three-dimensional plate). Semi-circular edges were chosen for the tests as it was thought that the flow along this shape would be less sensitive to small local incidences than would a shape of sharper form, such as a triangular edge. The 6 in. plate was sting-mounted with a single stabilizing strut from the tunnel wall to the plate axis just aft of the leading edge and on the opposite surface of the plate from that on which the measurements were to be taken. Both plates were tapped for pressure measurements along their centre-lines; the 6 in. plate on both surfaces, and the 'two-dimensional' plate on one surface only. Turbulence was stimulated on both plates with a 0·028 in. diameter wire stuck to the surface 4·61 in. from the leading edge.

The boundary-layer traverses were performed at standard chordwise distances from the leading edge and these are referred to as position numbers 1 to 7 in the text. Details of their location on the plate surface are recorded in Table 1.

The boundary-layer traverses were made with a Pitot tube (0·027 in. diameter) mounted on a remotely controlled traversing yaw-meter based on the instrument designed by Bryer[6]. Direct indication was available to 0·001 in. in translation and 0·1° in rotation. The interference of this traversing unit with the pressure distribution on the plates was larger than had been anticipated in the design stage and resulted in a maximum suction coefficient on the plate surface of the order of 0·04. This interference of the traversing unit also tended to cause a circulation around the plates which had a marked effect on the boundary-layer development on the plate surface; consequently, a wooden dummy traversing unit was constructed to match the drag of the main unit and this was mounted on rails facing the reverse side of the plate so that it could be moved in sympathy with the main unit. Thus, the pressure difference between the two surfaces of the plates (and hence across the longitudinal edges of the finite-span plate) was kept small; the maximum recorded value during a test being equivalent to $\Delta C_p = 0{\cdot}006$.

Great care was taken to ensure that the plates were aligned at zero incidence and yaw. However, all the tests were repeated with the 6 in. span plate at small incidence ($\pm 0{\cdot}23°$) and then at small yaw (0·76°) and, although showing interesting effects on the spanwise distributions, these tests showed incidence and yaw to have little effect on the final analysis. These latter tests are reported fully in Reference 1.

3. *The Experimental θ, C_f and H Distributions.*

The values of θ, C_f and the form factor H measured on the test plate are plotted in Figs. 1 and 2*. A number of corrections have been applied to these quantities and an account of these, including some comments on some details of the analysis of the data, is presented in Appendix I.

It is seen in these figures that all the distributions on the finite-span plate are not quite symmetrical about the centre-line. No explanation for this was evident from the tests as subsequent measurements with the plate at small yaw and small incidence indicated that this asymmetry could not be due to inadvertent angles of yaw and incidence. However, the amount of asymmetry is small and whatever its cause it is unlikely to affect the spanwise mean values of the quantities involved. It will be seen that apart from this slight asymmetry for any chordwise station there is a good measure of uniformity of the boundary-layer characteristics over the plate span except for regions close to the edges where an edge effect is evident.

* In these and later figures 3D stands for three-dimensional i.e. the data refer to the plate of finite span, 2D stands for 'two-dimensional'.

However, it is seen in Figs. 1 and 2 that the edge effect which is so well developed at the later chordwise positions does not appear to develop immediately aft of the trip wire. This is regarded as due to two factors; firstly, the presence of turbulent wedges from the corners of the leading edge result in the boundary layer at the trip wire being much thicker at the edges of the plate than at the centre-line so that the edge effect (as here understood) is somewhat masked in its early stages, although if there is an extensive laminar region the overall aspect-ratio effect may be enhanced by this factor (*see* Appendix II). Secondly, at the earlier chordwise positions the edge radius of the plate is large compared with the boundary-layer thickness ($\delta/R \ll 1$, R = edge radius of plate) so that the initial boundary-layer development along the curved edge is not very different from that of two-dimensional flow and the edge effect does not become fully evident until further back along the plate. This point is considered more fully in Section 4.1.

It is seen that the momentum defect on the plate surface spreads laterally off the edges of the plate and at the rearward chordwise positions the values of θ on the plate surface in the vicinity of the longitudinal edges are found to be lower than they would have been under truly two-dimensional development of the boundary layer. The value of H is also lower in these regions near the plate edges, whilst the measured values of C_f are higher than they would have been under two-dimensional conditions. Consequently, one may infer that the drag coefficient of the three-dimensional plate is higher than that of a two-dimensional plate of equivalent area. This point is more evident in the next section.

The quantities of momentum-defect flux off the edges of the three-dimensional plate cannot be meaningfully represented as a simple distribution of momentum thickness of θ extending the curves of Fig. 1 because the logical plane of integration to determine θ there is not obviously parallel to the normal to the main part of the plate. However, the quantities of momentum-defect flux measured in the boundary layer outside what are here referred to as the effective edges* of the plate are tabulated as a momentum area in Table 2. Two sources have contributed towards this momentum-defect flux, these are the lateral spread of momentum defect from the plate surface to beyond the effective edges and the effect of skin-friction stresses on the portions of the semi-circular edges outside the effective span. This breakdown of the momentum-defect flux off the edges of the plate according to its origin is important in assessing the degree to which the conditions at the edge of the actual plate approach those which would have been present had the plate been ideally thin and this point is considered further in Section 5.

4. *The Boundary-Layer Development along the Centre-line of the Finite-Span Plate.*

4.1. *Comparison with the 'Two-Dimensional' Plate.*

Townsend's concept[3] of an aspect-ratio effect was that of an effect over the whole span of the plate to which any effect which is limited to the edges is quite secondary. If this were so, the flow along the centre-line of the plate spanning the tunnel would not have been two-dimensional in

* The effective edge of the plate is here arbitrarily taken to be $R/2$ inboard of the geometric edge of the plate, where R is the radius of the edge; thus the effective plate span was 6·19 in. Later analysis (described in Section 5) of the similarity of flow in the edge regions for different chordwise positions lends support to the edges being taken at the junction of the flat-plate surface and the semi-circular edge. However, in what follows differences that can result from taking this latter position for the edge are small and do not affect the general discussion.

nature but, because the edges of the plate spanning the tunnel were immersed in the thick turbulent boundary layer of the tunnel walls, it would have been subjected to an edge effect in an opposite sense to that which affected the finite-span plate. The actual edge effect on the plate spanning the tunnel could therefore be expected to augment any differences which might have otherwise been present between the results from the two plates.

In Fig. 3, the values of θ measured along the centre-line of the finite-span plate are compared with those measured on the 'two-dimensional' plate, and the results are also given in Table 3. It is seen that, at both speeds tested, the boundary layers soon settle down from the slightly different conditions aft of the trip wire on the two plates and merge to common values of θ; in fact, any differences occurring towards the rear of the plate are within the measurement accuracy of θ. This suggests that the boundary-layer development along the centre-line of the finite-span plate was two-dimensional in nature, and this is confirmed strongly by the comparison of the velocity profiles measured on the two plates and presented in Figs. 4 and 5 where they are seen to become identical at the rearward plate positions.

It may be argued nevertheless that as the separate boundary layers reach similar conditions at the rear of the plate when they started from slightly different conditions aft of the trip wire, they may not both be obeying the same laws. However, if a Prandtl-Schlichting law for the growth of θ from the different conditions aft of the trip wire is assumed, and the values of θ are then calculated for the rearward plate positions, it is found that they differ by not more than one unit in the fourth decimal place. Hence, we can infer that both boundary layers are obeying the same law, although this is not necessarily exactly the same as the Prandtl-Schlichting law.

Consequently, we conclude that the flow along the centre-line of a plate of finite span is two-dimensional in nature at least until such a position that the edge effects have spread from the edges as far as the centre-line. We may note that this had not happened on the experimental plate tested which had an effective l/b ratio of $5 \cdot 4$.

4.2. *Comparison with Various Empirical Laws.*

In Fig. 6 the growth of momentum thickness for the boundary layer along the centre-line of the finite-span plate at one wind speed is compared with the predictions of four empirical laws, viz. Schoenherr, Prandtl-Schlichting, and the two relations proposed by Hughes, and the values of C_F calculated from the data for all the speeds tested are plotted in Fig. 7 against Reynolds numbers. The comparison was made by calculating for each law an apparent origin of turbulence for the boundary layer such that the values of θ calculated from the law agree with the measured values towards the rear of the plate. The comparison could equally well have been performed by matching values of θ towards the leading edge of the plate but it was felt for reasons that follow that the procedure adopted was physically more significant. It is seen in Fig. 6 that the experimental variation of θ did not conform exactly to any of the laws although the closest agreement is with the Prandtl-Schlichting law particularly towards the rear of the plate. It is shown in Reference 1 that the experimental values of θ reflect some over-stimulation of the boundary layer by the trip wire which resulted in abnormally high values of C_f at the early plate positions.* This over-stimulation makes any direct comparison of the measured θ growth with the standard laws inconclusive but it can have

* It is believed that the trip wire stimulates mixing a little downstream of it in excess of that in a naturally developing turbulent boundary layer. This results in a fuller velocity profile and a higher skin friction. Evidence for this is to be found in the low values of H (about $1 \cdot 31$) measured at position 1 (*see* Fig. 1).

little effect on the analyses described later, in which the spanwise data have been referred to the measured centre-line values.

A further basis of comparison between the measured boundary-layer growth and the empirical laws is the relationship between C_f and R_θ which is unique for each law. The distribution obtained from the present test results is plotted in Fig. 8 in which the over-stimulation of the boundary layer is apparent in the high values of C_f at the early plate positions. However, the boundary layer seems to have settled down somewhat by the rearward plate positions and it is interesting to note that, in these regions, the experimental points tend towards the Prandtl-Schlichting relation rather than towards the Hughes' relations.

5. *The Edge Effect on the Finite-Span Plate.*

5.1. *The Spread of the Edge Effect.*

It has been shown in Section 4 that the boundary-layer development along the centre-line of the finite-span plate tested was the same as on the two-dimensional plate. Hence it can be argued that the effect of the longitudinal edges in producing low values of θ and H and high values of C_f in the vicinity of these edges is the whole of the aspect-ratio effect and is not secondary and additional to some effect which is present across the whole span. The edge effect is seen, in Figs. 1 and 2, to grow from the edges towards the centre-line with increasing chordwise distance and, once the effect has settled down, appears to spread in such a way that the distributions near the edges are of similar shape. This feature is considered further in Section 6 and is used to extend the range of usefulness of the present data. The portion of the span affected by the edges is roughly a boundary-layer thickness in width from each edge; thus, these effects can be expected to meet on the centre-line of the plate when the half-span of the plate is approximately equal to the boundary-layer thickness on the centre-line; this is also considered further in Section 6.

5.2. *The Drag of the Finite-Span Plate.*

It is apparent in Fig. 2 that, as values of C_f in regions affected by the edges of a three-dimensional plate are higher than those on the centre-line (which are the equivalent two-dimensional values), the drag of a finite-span plate is higher than that of a corresponding area under two-dimensional flow conditions; here, it is proposed to calculate the magnitude of this effect for the experimental plate and to make some initial allowance for the fact that the thickness of the plate was not infinitesimal.

Two sets of results are available for calculating the drag of the finite-span plate, namely the direct measurement of the momentum-defect flux across the span of the plate at particular chordwise positions, and the measurements of skin friction which may be integrated chordwise and spanwise up to a particular chordwise position to give the drag of the plate up to that chordwise position. These two methods should agree if all the quantities involved were accurately measured, but possible, if small, inaccuracies involved in the measurement of skin friction or the estimation of the momentum-defect flux off the edges of the plate made it impossible to assess which method was the more reliable. Hence, both methods were used and the results compared. However, let us first consider the corrections to be made to these calculations to allow for the effect of plate thickness.

We have seen that the edge regions of a three-dimensional plate are regions of higher shear stresses than the centre-line. An ideally thin plate would have zero edge area subjected to these high stresses so that no contribution to the momentum-defect flux can arise from its edge area. However, the actual plate tested has an edge area of significant magnitude subjected to these high stresses so

that, even if the edge area is included in the total area used to reduce the drag to coefficient form, this edge area makes a direct contribution to the fact that the spanwise mean drag coefficient is higher than the equivalent two-dimensional value. The measured values of drag coefficient may be adequately corrected for this by excluding from the total spanwise drag any which originated in the action of skin-friction stresses on the edge areas. Here the edge areas are defined as the surface area of those portions of the semi-circular edges lying beyond the effective edges of the plate. In the integration of C_f this is simply done by excluding these edge areas from the spanwise integration. In the spanwise integration of the measured values of θ, an estimate of the amount of momentum-defect flux due to the edge areas was made from an integration of the values of C_f measured on the edge over the edge areas and this momentum-defect flux was then subtracted from the total quantity. With these corrections, the two methods for calculating the plate drag give that due to the action of skin-friction stresses on the plate surface only. However, these results cannot necessarily be taken to apply to an ideally thin plate although they are a useful guide. Apart from possible if small effects arising from the presence of initial turbulence wedges from the corners ahead of the trip wire (*see* also Appendix II) there is an important effect related to the ratio of the boundary-layer thickness to the radius of the edge of the plate. This effect will be considered further in Section 7 but for the present we will not take it into account.

The aspect-ratio effect calculated from the experimental data by the methods mentioned above allowing for the frictional stresses acting on the edge areas is presented in Table 4 in the form of resistance ratios, viz. the ratio of the C_F of the 3D plate to that of the 2D plate ($r = C_F/C_{F\,0}$). The values in the first and third columns were calculated from the measured momentum defect, and those in the second and last columns were calculated from the skin-friction measurements. Also, to indicate the effect of thick edges, Table 5 has been included in which the resistance ratios are uncorrected for the edge-area frictional stresses. It is seen that these ratios are somewhat higher than those of Table 4 as is to be expected but that the difference is small. Conversely if the effective edges were taken coincident with the edges of the flat part of the plate (from the work described later this would seem on the whole the preferred position) the resulting resistance ratios would be a little smaller (by about $0{\cdot}002$) than the values given in Table 4.

A breakdown of the momentum-defect flux present at a chordwise position is presented in Fig. 9. Here $(\Delta + E)$ is the total drag presented as a mean momentum thickness, Δ is the contribution due to the measured momentum-defect flux over the effective span of the plate surface, E is the contribution over the edge areas and Z is the contribution due to the frictional stresses acting on the edge areas. It is seen how difficult it is to calculate the aspect-ratio effect accurately because this effect only appears as a small difference $[(\Delta + E - Z) - \theta_c]$ of large terms which were measured separately.

If we revert to Table 4 we see that there is an overall measure of agreement between the two methods of calculation of the resistance ratio and this leads to the important conclusion that we can use either the momentum-defect or skin-friction measurements with fair confidence. The actual measurements of momentum-defect flux and the corresponding integrals of the measured skin friction also showed very good agreement, the differences being well within 5% and with a mean of about 2% (*see* Appendix I). Values of r towards the leading edge are sensitive to any non-uniformities in the distribution of θ aft of the trip wire and in particular to the effects of the transition wedges from the corners but at the rearward stations these non-uniformities have been smoothed out and the values of 'r' quoted may be taken as more closely applying to the aspect-ratio effect. This effect of aspect ratio is much smaller than that required by Hughes[2], thus, at the rear of the plate with an

effective l/b ratio of 5·4 the value of 'r' is about 1·019 whilst the value required by Hughes' formula is about 1·08. However, as already noted we have a further effect to take into account before we can generalise from these results.

6. *Analysis of the Similarity of the θ and C_f Distributions near the Edges.*

In Section 5.1 it was mentioned that the spanwise distribution of the boundary-layer parameters near the edges of the three-dimensional plate appear to be similar in shape at the later chordwise positions. The dotted lines on Fig. 1 roughly define the region of strong edge effect and they indicate an inward rate of spreading which is proportional to the centre-line value of θ and it will be seen that they intersect the distributions in corresponding parts of each distribution. Hence, it appears that the lateral scale defining the shape of these edge distributions is proportional to some chordwise scale which is, at least, closely related to the centre-line value of θ. Two scales suggest themselves, one is indeed the centre-line value of θ, and the other is simply the chordwise distance x, with both measured from some suitable origin for the start of the spread of the edge effect. As the lateral spread of the edge effect is a momentum transfer process, it seemed likely that it should be dependent on Reynolds number in much the same way as the centre-line growth of θ so that θ_c was the scale favoured for the analysis of the test results. However, Hughes' analysis of his results implied that the chordwise distance (x) was the correct lateral scale[2] so that the present results were analysed using both scales and the results compared.

The origin from which the edge effect appears to have started spreading is an important factor in the investigation of the similar shapes of the edge distributions and it is not immediately obvious from Fig. 1 just what this origin should be. The degree of 'similarity' shown by the distributions in Fig. 1 in relation to the dotted lines suggest that the origin of the edge effect is the apparent origin of turbulence ($\theta=0$); it is certainly plausible that the amounts of momentum defect on and off the edge of the plate should be simply related. A number of other possible origins were tried in the analysis of the data, but the best results for both the lateral scales considered, viz. θ and x, were obtained with an origin at the apparent origin of turbulence and only these results are presented in this report.

Thus after a number of possibilities were examined the closest similarity of the shapes of the distributions of the boundary-layer parameters for chordwise stations 4 to 7 was obtained by plotting

$$\frac{C_f - C_{fc}}{C_{fe} - C_{fc}} \text{ and } \frac{\theta_c - \theta}{\theta_c - \theta_e} \text{ against } \frac{z - z_0}{\theta_c} \text{ or } \frac{z - z_0}{x - x_0} \tag{1}$$

where θ_e, C_{fe} are the values of θ and C_f respectively, at the edge of the plate, $z - z_0$ is the inboard distance from each edge of the plate measured from a datum z_0 which is taken to be the junction of the flat part of the plate and the semi-circular edge, and $x - x_0$ is the chordwise distance from the apparent origin of turbulence. The resulting graphs are seen in Figs. 10 and 11. A good collapse of the separate distributions has been achieved so that a measure of similarity in the edge distributions is evident. On the whole, the collapse obtained using θ_c as the length scale is slightly better than that obtained using 'x'.

7. *The Drag of a Finite-Span Plate Deduced from the 'Similarity' Analysis.*

The mean spanwise drag coefficient up to any particular chordwise position is

$$C_F = \frac{1}{bx} \int_0^x \left[\int_{-b/2}^{b/2} C_f dz \right] dx. \tag{2}$$

If the 'z' wise integration is applied to the spanwise C_f distributions of Fig. 2, and the two 'similarity scales' of θ_c and x are applied to the difference $C_f - C_{fc}$, the spanwise mean values of C_f are, respectively

$$\langle C_f \rangle = C_{fc} + 2\theta_c C_{fc} \left(\frac{C_{fe}}{C_{fc}} - 1 \right) \frac{I}{b}, \tag{3}$$

$$\langle C_f \rangle = C_{fc} + 2C_{fc} \left(\frac{C_{fe}}{C_{fc}} - 1 \right) \frac{xI'}{b}, \tag{4}$$

in which I and I' are the areas under the curves of Fig. 11a and b and have the numerical values of $6{\cdot}9$ and $0{\cdot}0145$ respectively.

Then, on integrating from 0 to x with the assumption that C_{fe}/C_{fc} is constant (*see* below) we get:

$$\frac{C_F}{C_{F0}} = \frac{C_F}{C_{Fc}} = 1 + \frac{I}{2} \left(\frac{C_{fe}}{C_{fc}} - 1 \right) C_{F0} \frac{x}{b} \tag{5}$$

for 'similarity' based on θ, and, with $C_{fc} \propto R_x^{-1/5}$

$$\frac{C_F}{C_{F0}} = 1 + 0{\cdot}89I' \left(\frac{C_{fe}}{C_{fc}} - 1 \right) \frac{x}{b} \tag{6}$$

for 'similarity' based on 'x'. It will be noted that an important difference between equations (5) and (6) is that the former includes a Reynolds number effect in the form of the factor C_{F0} in its right-hand side.

We next require to examine the value of the ratio, C_{fe}/C_{fc}, which has, in the analysis above, been assumed to have a constant value. The variation obtained in the present tests is presented in Fig. 12 and in the interpretation of this graph we have again to consider the effect of the finite thickness of the plate. As indicated in Section 5.2 the finite thickness of the plate has two effects on the conditions at the edge of a three-dimensional plate. There is first the effect already considered, namely the direct effect in which this edge thickness provides additional edge area to sustain the high edge skin-friction stresses. The second effect which we now consider is that which affects C_{fe}/C_{fc} and is due to the fact that when the boundary layer is thin compared with the edge radius of the plate ($\delta/R \ll 1$), the boundary-layer development along the edge shape tends to be much the same as that along a two-dimensional flat plate and, consequently, much the same as that along the centre-line of the three-dimensional plate: i.e. there is little edge effect and $C_{fe}/C_{fc} \simeq 1{\cdot}0$. Further back along the plate the true edge effect becomes increasingly evident as δ/R increases and with it C_{fe}/C_{fc} increases. For large enough δ/R we may expect C_f/C_{fc} to tend to the value appropriate to an ideally thin plate.

The degree to which the edge conditions on a thick plate approach those on a thin plate is indicated by the proportion of the rate of increase with x of the momentum-defect flux off the edge of the plate which was directly due to the edge area. If it is a negligible proportion, the conditions will conform to those on a thin plate. This criterion for the present data is illustrated in Fig. 13 in which E is the total momentum defect in the region of the edges and Z is that due to the extra edge areas alone. It is seen that the rate of growth of $(E-Z)$ with x was several times that of Z towards the rear of the plate. Consequently, although the value of C_{fe}/C_{fc} had not developed fully

to a value approximate to an ideally thin plate it had presumably gone a fair way towards it.* The trend in Fig. 12 suggests that the ultimate value of C_{fe}/C_{fe} is a constant in the range $1{\cdot}2 \rightarrow 1{\cdot}3$, although it might possibly be a slowly varying function of Reynolds number. With $C_{fe}/C_{fc} = 1{\cdot}2$ the expressions for the resistance ratios become

$$C_F/C_{F0} = 1 + 0{\cdot}69C_{F0}x/b \tag{7}$$

$$C_F/C_{F0} = 1 + 0{\cdot}0026x/b, \tag{8}$$

while, if C_{fe}/C_{fc} is taken as $1{\cdot}3$ the resistance ratios become:

$$C_F/C_{F0} = 1 + C_{F0}x/b \tag{7a}$$

and

$$C_F/C_{F0} = 1 + 0{\cdot}0039x/b. \tag{7b}$$

An important deduction from this analysis is the position on the plate centre-line at which the edge effects would begin to meet. The distributions of θ and C_f of Figs. 10 and 11 both indicate edge effects beginning at $z - z_0 \simeq 15\theta_c$ from the plate edge so that the plate breadth for the start of centre-line interaction would be

$$b \simeq 30\theta_c \tag{9}$$

On the basis of 'similarity in x', the critical plate proportions at the Reynolds number of the present tests are given by

$$l/b \simeq 16. \tag{10}$$

8. *Comparison with Previous Work.*

The most important previous investigation of this subject has been the overall drag measurements of Hughes,[2] the only edge measurements being those of Allan and Cutland[7] and those reported by Townsend.[2]

The results of Ref. 7 show the same edge behaviour as the present tests but show also some change of θ_c in the wake of a 50 ft towed plank between draughts of 57 in. and 25 in. However, from equation (9) the edge effect would spread inward by about 12 in., so there is no obvious inconsistency with the present tests.

Townsend reports measurements of edge distributions which are similar to those of the present work and which result in an expression for the resistance ratio of

$$r = 1 + 0{\cdot}002l/b \tag{11}$$

which compares favourably with equation (8). However, he considers this direct effect of the edges to be secondary to a further, unmeasured effect of aspect ratio which affects the whole span, whereas the present work shows it to be the whole effect.

The difference between the magnitude of the edge effect predicted by Hughes and that calculated from the present results is in general so large as to warrant a closer look at Hughes' analysis of his work.

---

* It may be noted that for Fig. 13 the values of E and Z are determined for effective plate edges at $R/2$ beyond the junction of the flat part of the surface and each semi-circular edge as in Section 2. However, a change of effective edge position can only result in roughly the same changes in E and Z for any given chordwise station so that the argument given here is independent of the effective edge position assumed.

In Fig. 10 of Reference 2, the resistance ratios (C_F/C_{F0}) calculated by Hughes from his various tests using his basic two-dimensional skin-friction law are plotted against l/b, and it is concluded from the dispersion which appears above $l/b = 2{\cdot}0$ that edge effects begin to meet significantly on the centre-line at this value of l/b. The present work shows this not to be so and a further reason has to be found for this dispersion. Now, each point on Hughes' Fig. 10 represents data covering a range of Reynolds numbers which is very large; consequently, in order to see if the differences occurring in his Fig. 10 are genuine and not simply introduced by the smoothing processes which defined each point, it is instructive to plot a graph corresponding to Hughes' Fig. 10 but in which every single test is plotted instead of the smoothed results of test series. Such a graph is Fig. 14 of this paper. It is seen that the scatter within test series (l/b = const.) is equally as great as the differences between the lines on Hughes' Fig. 10, and the trend of points no longer passes smoothly through the origin.

In Fig. 14 the points have been identified with their test parameters (plate or pontoon, high, medium or low Reynolds numbers), and it is seen that at low values of l/b there is a distinct difference between the plate and pontoon results, in that the latter tend to lie near $C_F/C_{F0} = 1{\cdot}07$ for $l/b \to 0$ instead of falling rapidly to unity like the plate results. This could have been due to differences between the degree of leading-edge stimulation on the plates and pontoons (the effect of which is discussed in Appendix II), but could also have included a Reynolds number effect common to both because, for both, the higher Reynolds number results (denoted by symbols $\times$, $\perp$) are generally higher than those at lower Reynolds numbers. In any case these differences raise doubts as to the validity of Hughes' basic skin-friction law, the results suggest that there was a possible error of about 7% for at least some of the conditions tested.

The present work indicates such a small effect of aspect ratio on C_F that the older established empirical skin-friction laws need little, if any, correction to allow for its presence in the original tests which defined these laws. Consequently, Hughes' data were re-analysed using the Schoenherr law to give values for C_{F0} and the results are plotted in Fig. 15. It is seen that at higher values of l/b there is a significant divergence between results at high and low Reynolds numbers ($\times$, $\perp$ respectively). This could be due to the unsuitability of the Schoenherr law, or it could be the effect of C_{F0} acting on the resistance ratio in accordance with equation (5). To test the latter possibility the resistance ratios were plotted against $(l/b)C_{F0}$ and Fig. 16 was produced. This plot is a marked improvement over the corresponding plots of Figs. 14 and 15 in that the points from both the plate and pontoon tests collapse better on to a straight line through the origin, and there are no longer any marked trends with Reynolds number. This indicates that Hughes' data fit well into the pattern of the older established empirical skin-friction laws if the edge effect is analysed according to equation (5) and not equation (6), i.e. on a similarity law of the edge effects based on the centre-line θ and not on x.

In Fig. 16 the trend of points near $(l/b)C_{F0} = 0$ cuts the axis not far from $r = 1{\cdot}0$, which suggests that the Schoenherr skin-friction law is quite a satisfactory description of C_{F0} on a two-dimensional flat plate. However, the precise intersection with the axis is not clear; the trend at higher values of $(l/b)C_{F0}$, if extrapolated to $(l/b)C_{F0} = 0$, passes through the origin, but the points near $(l/b)C_{F0} = 0$ favour an intersection at about $0{\cdot}98$; the difference of this value from unity could be due to experimental errors and departure from fully turbulent flow or due to the analysis but in any case it is small.

A line through the origin which gives a reasonable fit to the points of Fig. 16 is

$$r = 1 + 0{\cdot}8(l/b)C_{F0}. \tag{12}$$

If we assume that the effective origin of the ordinate of Fig. 16 should be at 0·98 and not 1·00 on the grounds that the trend of the points near the origin indicate an error in the basic Schoenherr skin-friction law of the order of 2%, then a good fit will be

$$r = 1 + (l/b)C_{F0} \tag{13}$$

If we compare equations (12) and (13) with the corresponding equations (7) and (7a) resulting from the present work

$$r = 1 + 0{\cdot}69(l/b)C_{F0}, \text{ for } C_{Fe}/C_{Fc} = 1{\cdot}2 \tag{7}$$

and

$$r = 1 + (l/b)C_{F0}, \text{ for } C_{Fe}/C_{Fc} = 1{\cdot}3 \tag{7a}$$

we see that the level of agreement is good. Bearing in mind the great range of parameters covered by Hughes' experiments one can infer that equation (13) or (7a) can be regarded as a reliable guide to the aspect-ratio effect for general use and predictions based on this equation are unlikely to underestimate the effect. As an example, we may note that for the plate of the present experiments equation (13) predicts that $r = 1{\cdot}020$ at 85 ft/sec, whilst the measurements of C_f gave $r = 1{\cdot}016$ for the appropriate effective plate span.

The magnitude of this edge effect is however so small that the older established skin-friction laws need not be suspect on account of it and need not be drastically modified as suggested by Hughes. For example, an analysis of the data on which the Schoenherr law is based shows that the magnitude of the possible error due to aspect-ratio effect is never more than 3 to 4% and is generally within the order of differences to be found between the values of C_{F0} predicted by different laws. We conclude that the drag data from Hughes' tests can now be unified with the host of wind-tunnel data on flat-plate drag and with the results of semi-mathematical analyses based on the boundary-layer velocity profile in supporting a basic skin-friction law which is not far removed from the Schoenherr or Prandtl-Schlichting laws.

9. *Conclusions.*

The present work has shown that the flow along the centre-line of a three-dimensional plate with a turbulent boundary layer is two-dimensional in nature until such a chordwise position is reached that the edge effects, which spread inwards from the longitudinal edges of the plate, meet on the centre-line. This occurs when the value of θ_c is about one thirtieth of the span, for the Reynolds numbers of the present tests, this corresponds to an l/b ratio of about 16. On regions of the plate surface affected by the edges, values of θ and H decrease laterally from their values in the unaffected spanwise areas to minimum values at the edges of the plate. At the same time, values of C_f in these regions are higher than in two-dimensional flow. The relationship between the value of C_f at the edge of a thin plate and its centre-line (two-dimensional) value was not completely defined by the present tests because conditions at the edge of the plate never developed sufficiently to eliminate the effect of plate thickness. The experimental values of C_{fe}/C_{fc} increased from about unity at the front of the plate to almost 1·2 at the rearward positions. The initial rate of increase of C_{fe}/C_{fc} was large but the variation towards the rear was much slower and it seemed reasonable to assume that for an ideal thin plate the ratio would become a constant value somewhat higher than 1·2 or possibly a slowly varying function of Reynolds number. A re-consideration of Hughes' drag data in the light of the present work suggests that the ratio should be taken as 1·3.

The edge regions of the plate in which the flow is affected by the presence of the edges has been shown to spread on to the plate surface with a measure of similarity for different chordwise stations

such that the lateral length scale defining the amount of spread is θ_e. This concept that the lateral distributions of the boundary-layer parameters near the edges of the plate are similar has been applied to yield a formula for the aspect-ratio effect on the drag of a thin plate. The result of this analysis is that the resistance ratio of a three-dimensional plate can be represented by

$$C_F/C_{F0} = 1 + 3{\cdot}45(C_{fe}/C_{fc} - 1)(l/b)C_{F0}.$$

Hughes' data for the drag of plates and pontoons towed in a ship tank have been re-analysed using this form for the aspect-ratio effect. This differs from his own analysis which was based on

$$C_F/C_{F0} = 1 + \text{const.} \times l/b.$$

This re-analysis presents Hughes' data with less scatter than formerly and results in an edge effect which is consistent with the present work and is very much smaller than Hughes' own predictions. The recommended expression for the resistance ratio in the light of Hughes' data and that of this present work is

$$C_F/C_{F0} = 1 + (l/b)C_{F0}.$$

This aspect-ratio effect is sufficiently small to permit the conclusion that the older established empirical skin-friction laws, such as the Prandtl-Schlichting or Schoenherr laws, do not include much error due to it and may still be accepted with an accuracy adequate for most engineering purposes as describing the skin-friction drag of a two-dimensional flat plate. We note finally that for a plate of finite thickness the thickness effects would tend to reduce somewhat the effect of aspect ratio on the resistance ratio.

LIST OF SYMBOLS

b	Span of 3D plate
C_f	Local skin-friction coefficient
C_F	Mean or overall skin-friction coefficient
C_p	Pressure coefficient $(p-p_s)/\frac{1}{2}\rho V^2$
r	Resistance ratio (C_f for 3D Plate)/(C_f for equivalent 2D Plate)
R	Radius of semi-circular edge to plate
R, R_x	Reynolds numbers
l	Length of plate
x	Chordwise distance on plate
z	Spanwise distance measured inboard from datum
θ	Momentum thickness
δ^*	Displacement thickness
δ	Boundary-layer thickness
3D	Finite span or three-dimensional
2D	Two-dimensional
P.E.	Port edge of plate (viewed along working surface)
S.E.	Starboard edge of plate (viewed along working surface)
Δ	Contribution to measured momentum-defect flux over plate effective span
E	Contribution to measured momentum-defect flux over edge areas
Z	Contribution to measured momentum-defect flux due to frictional stresses on edge areas

Suffices

e	Longitudinal edge of plate
c	Centre-line of plate
0	Value for infinite aspect ratio

REFERENCES

No.	*Author(s)*	*Title, etc.*
1	E. B. Davies	Edge Effects in Turbulent Boundary Layer Flow on a Three-dimensional Flat Plate. (Thesis presented for Ph.D. degree, University of London. 1961.)
2	G. Hughes	Friction and Form Resistance in Turbulent Flow, and a Proposed Formulation for use in Model and Ship Correlation. *Trans. Instn. Nav. Archit.*, Vol. 96, No. 4. October, 1954.
3	A. A. Townsend	On the Turbulent Boundary Layer on a Flat Plate of Finite Width. A.R.C. 16 618. March, 1954.
4	J. H. Preston	The Determination of Skin Friction by means of Pitot Tubes. *J. R. Ae. Soc.*, Vol. 58. 1954.
5	E. F. Relf, R. C. Pankhurst and W. S. Walker.	The Use of Pitot Tubes to Measure Skin Friction on a Flat Plate. A.R.C. 17 025. August, 1954. (Combined with other papers in A.R.C. R. & M. 3185.)
6	D. W. Bryer	A Remotely-Controlled Traversing Yawmeter for Boundary Layer Exploration. A.R.C. 16 218. October, 1953.
7	J. F. Allan and R. S. Cutland	Wake Studies of Plane Surfaces. *Trans. N.E. Coast Instn. Engrs. Shipb.*, Vol. 69. February, 1952.
8	A. Fage	Note on Report A.R.C. 17 025 (Ref. 5). A.R.C. 17 320. January, 1955.
9	V. M. Falkner	A New Law for Calculating Drag. *Aircraft Engineering*, Vol. XV. March, 1943.

APPENDIX I

Analysis and Corrections of the Experimental Results

1. *Pitot-Tube Displacement Effect.*

The velocity profiles in the boundary layer on the plate surface were measured with a pitot tube of diameter 0·027 in. The correction for tube displacement was taken to be that determined by McMillan and equal to $(0{\cdot}15 \times 0{\cdot}027) = 0{\cdot}004$ in. This ignores the effect of the wall, but it was shown that the correction for turbulence and the effect of the wall are of similar magnitudes and tend to cancel one another out. Consequently, the measured velocity profile was corrected by adding 0·004 in. to all the ordinates, or by adding $(0{\cdot}004 \times 0{\cdot}25) = 0{\cdot}001$ in. to the values of θ calculated from the experimental profiles.

2. *Traversing-Gear Interference.*

The interference of the traversing gear with the pressure distribution on the surface of the plate was not small and resulted in an acceleration of the flow up to the measurement position. A correction was applied to the measured values of θ and C_f to allow for this and also to allow for the slight differences between the effective wind speed in any particular test and the nominal wind speed. This correction was not large and had a maximum effect of reducing θ by 5% towards the trailing edge of the plate, and increasing C_f by 1% at the same position.

3. *Accuracy of the Measured Values of C_f.*

Skin friction was measured using Prof. Preston's surface-tube technique in which the reading of a pitot tube when lying on a surface is taken to be a measure of the local skin friction. This technique requires that the tube's effective centre be in the part of the velocity profile where the logarithmic law (the 'law of the wall')

$$\frac{u}{u_\tau} = A \log \frac{yu_\tau}{\nu} + B \tag{AI.1}$$

is valid. However, the calibration to be used with the technique is related to the values of the constants A and B and there is not complete agreement as to their values. Further in the present tests the technique was applied to the flow near the edge of the plate where the three-dimensional perturbations to the boundary-layer flow might have affected the logarithmic profile sufficiently to invalidate the two-dimensional flow calibration. The velocity profiles were therefore analysed to see how far they conformed to equation (AI.1), also the calculated values of $\frac{1}{2}C_f$ were integrated from a datum value of momentum defect at the first measurement position to a general chordwise position and the result compared with the momentum-defect flux actually measured at that chordwise position. The calibration which gave the best agreement was that of the National Physical Laboratory

$$C_f = 0{\cdot}0592 C_p^{7/8} R_d^{-1/4} \tag{AI.2}$$

in which $C_p = (p_t - p_s)/\frac{1}{2}\rho V^2$ (p_t = pressure measured by the surface tube) and R_d is the Reynolds number based on the pitot-tube outside diameter. The difference obtained between the integrated C_f distribution and the measured momentum defect was generally well within 5% with a mean

of about 2% and no noticeable effects were introduced by the three-dimensional nature of the flow near the edges of the plate. The values of A and B which best matched the experimental velocity profiles were those of Fage[8], viz. 5·55 and 4·6.

4. *Analysis of Data.*

The analysis of the experimental data was by means of a digital computer and all integrations were performed using the trapezoidal rule or a parabolic formula. Samples of these calculations were checked against graphical integration and the error was generally less than $\frac{1}{4}$% but errors of 1% were approached for the spanwise mean value of θ when the plate was at yaw or negative incidence.

APPENDIX II

The Effect of Edge Stimulation of Transition in Enhancing the Aspect-Ratio Effect on the Drag of a Three-Dimensional Plate

Although it has been shown in the main text that it was not necessary to consider leading-edge stimulation effects to bring Hughes' drag data in line with the older established skin-friction laws, the effect of incomplete leading-edge stimulation on the apparent magnitude of the aspect-ratio effect is of practical interest and is simple to understand in a qualitative manner.

If the boundary layer near the leading edge is transitional in nature, the boundary layer in the vicinity of the longitudinal edges of the plate becomes turbulent much sooner than that on the rest of the plate span. This may be due to the leading-edge corners or due to the unstable 'wake' velocity profile in the flow outside the edges of the plate, but is always observed as the familiar turbulent wedges from the leading-edge corners. The drag of the edge portion of the plate is, consequently, increased above the two-dimensional value not only through the aspect-ratio effect but also through the earlier transition in these regions. Thus, at any particular value of the aspect ratio, the resistance ratio $\{(C_F)_{3D}/(C_F)_{2D}\}$ is higher than it would have been without any transition effect and the effect of incomplete leading-edge stimulation is to cause the slope of the graph of resistance ratio against l/b to be greater than it would have been under the action of a pure aspect-ratio effect, particularly for small l/b.

The magnitude of this transition effect will naturally vary with the length of laminar boundary layer, but an illustration is provided by the drag data of Gebers and Baker reported by Falkner[9] and reproduced here as Fig. 17. Gebers' tests were performed with a leading edge which strongly stimulated the boundary layer, in contrast to the leading-edge design in Baker's tests. It is seen in Fig. 17 that, at the higher Reynolds numbers at which turbulence would have been expected to have been stimulated near the leading edge on both plates, there is a measure of agreement in the aspect-ratio effect calculated from both sets of data. However, at lower Reynolds numbers the data from Baker's tests indicate a much higher aspect-ratio effect in contrast with Gebers' results which maintain a general low level. This is undoubtedly due to the existence of an appreciable length of transitional boundary layer near the leading edge of Baker's plate.

TABLE 1

Chordwise Location of the Standard Measurement Positions

Position No.	Distance from Trip Wire in inches	
	2D plate	3D plate
1	2·19	2·18
2	3·38	3·37
3	6·00	5·94
4	9·04	9·00
5	14·81	14·75
6	23·10	23·06
7	29·27	29·20

TABLE 2

Momentum-Defect Area outside the Effective Edges of the 3D Plate

Position No.	Momentum Defect in in.^{2}				
	85 ft/sec		106 ft/sec		
	S.E.	P.E.	S.E.	P.E.	
1	0·0032	0·0040	0·0032	0·0033	S.E.— Starboard Edge.
2	0·0040	0·0045	0·0041	0·0048	
3	0·0056	0·0059	0·0050	0·0059	
4	0·0068	0·0082	0·0086	0·0082	P.E.— Port Edge.
5	0·0130	0·0140	0·0116	0·0123	
6	0·0204	0·0210	0·0169	0·0210	
7	0·0262	0·0311	0·0235	0·0303	

TABLE 3

Comparison of θ on the centre-line of the 3D Plate with that on the 2D Plate

Position No.	85 ft/sec		106 ft/sec	
	$\theta \sim$ 3D plate	$\theta \sim$ 2D plate	$\theta \sim$ 3D plate	$\theta \sim$ 2D plate
1	0·0158	0·0163	0·0153	0·0160
2	0·0187	0·0198	0·0186	0·0193
3	0·0247	0·0255	0·0239	0·0245
4	0·0321	0·0325	0·0312	0·0312
5	0·0428	0·0441	0·0425	0·0424
6	0·0593	0·0589	0·0569	0·0566
7	0·0701	0·0701	0·0666	0·0668

TABLE 4

Experimental Values of the Resistance Ratio for the 3D Plate corrected for Frictional Stresses Acting on Edge Areas (Effective Span = 6·19 in.)

Position No.	85 ft/sec		106 ft/sec	
	$r^{(1)}$	$r^{(2)}$	$r^{(1)}$	$r^{(2)}$
1	1·033	1·034	1·035	1·035
2	1·033	1·027	1·028	1·024
3	1·022	1·021	1·022	1·017
4	1·011	1·015	1·013	1·018
5	1·017	1·013	1·005	1·015
6	1·011	1·017	1·001	1·016
7	1·021	1·019	1·015	1·018

(1) Calculated from the Measured Momentum Defect.

(2) Calculated from the Integration of C_f.

TABLE 5

Experimental Values of the Resistance Ratio for the 3D Plate Uncorrected for the Frictional Stresses Acting on Edge Areas

Position No.	85 ft/sec	106 ft/sec
1	1·041	1·041
2	1·032	1·032
3	1·024	1·023
4	1·019	1·022
5	1·019	1·019
6	1·022	1·021
7	1·023	1·023

Calculated from the Integration of C_f.

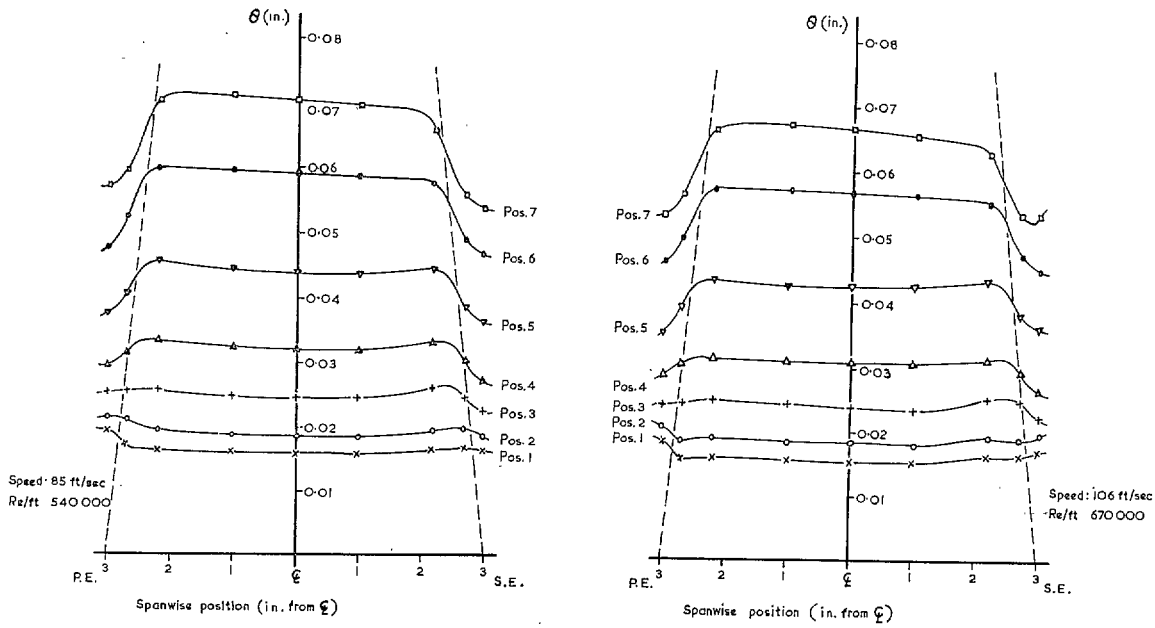

FIG. 1. Spanwise distribution of θ on the 3D plate.

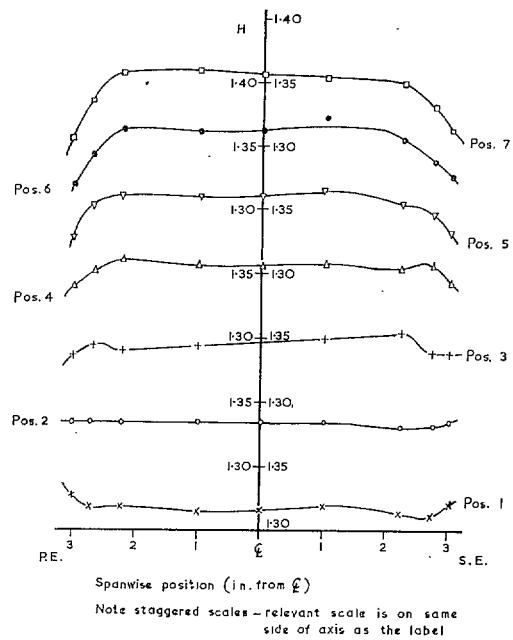

FIG. 1—*continued.* Spanwise distribution of H on the 3D plate—Speed 85 ft/sec.

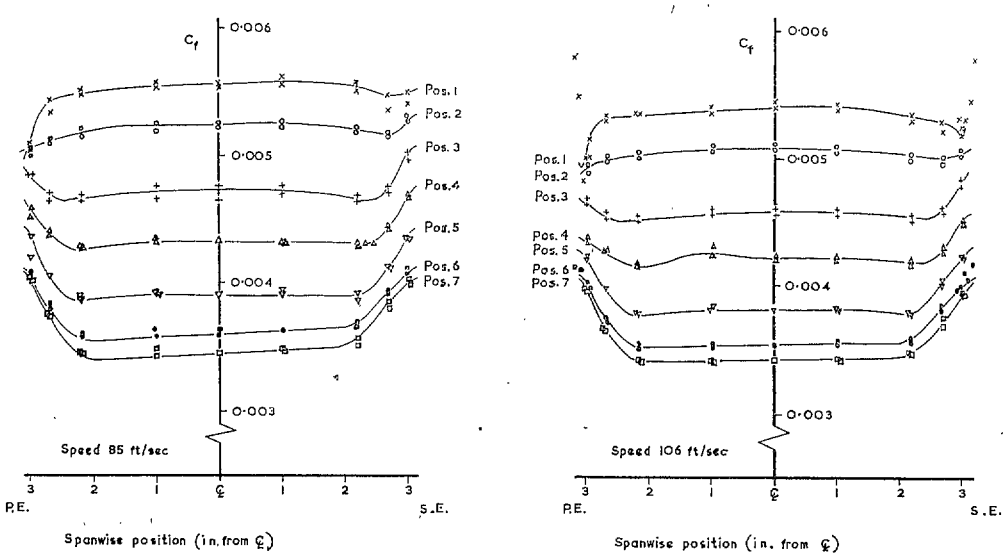

FIGS. 2a and b. Spanwise distribution of C_f on the 3D plate.

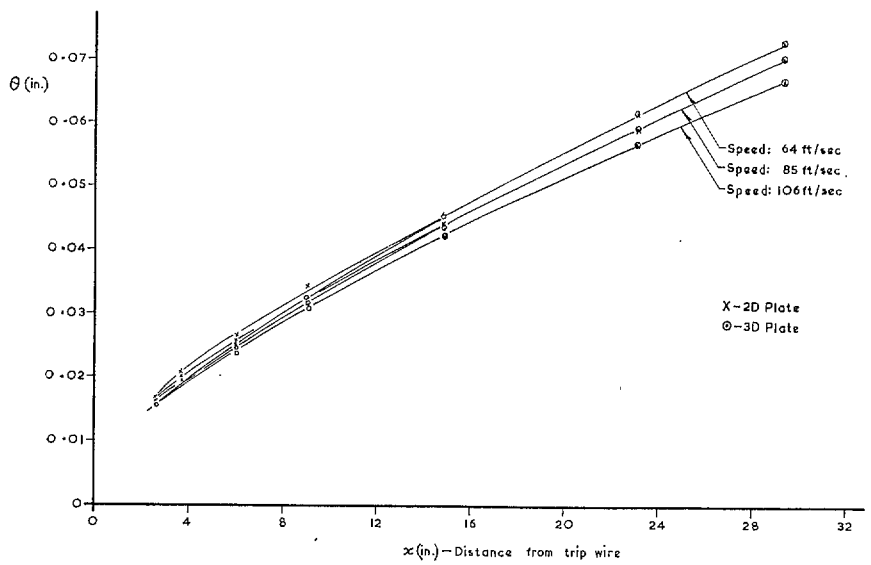

FIG. 3. Momentum-thickness growth on the 2D plate compared with that on the centre-line of the 3D plate.

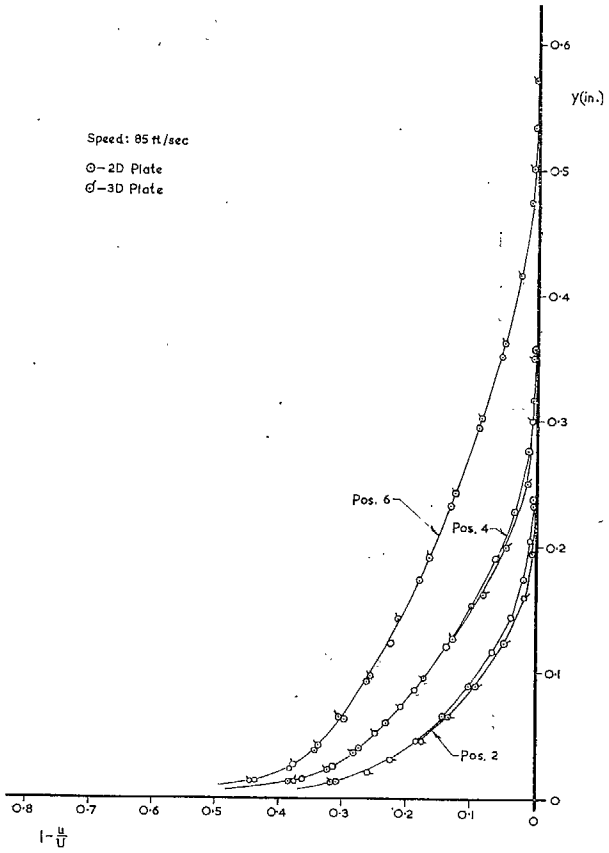

FIG. 4. Velocity profiles on the 2D plate compared with those on the centre-line of the 3D plate.

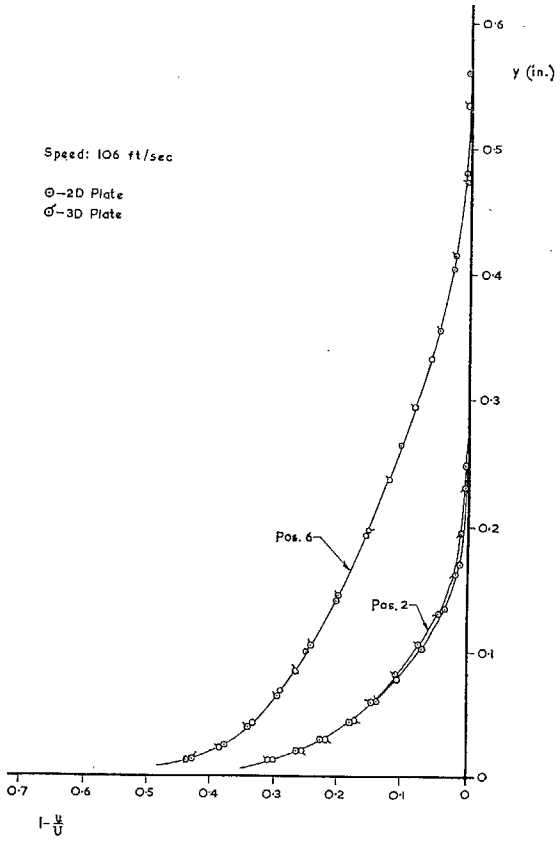

FIG. 5. Velocity profiles on the 2D plate compared with those on the centre-line of the 3D plate.

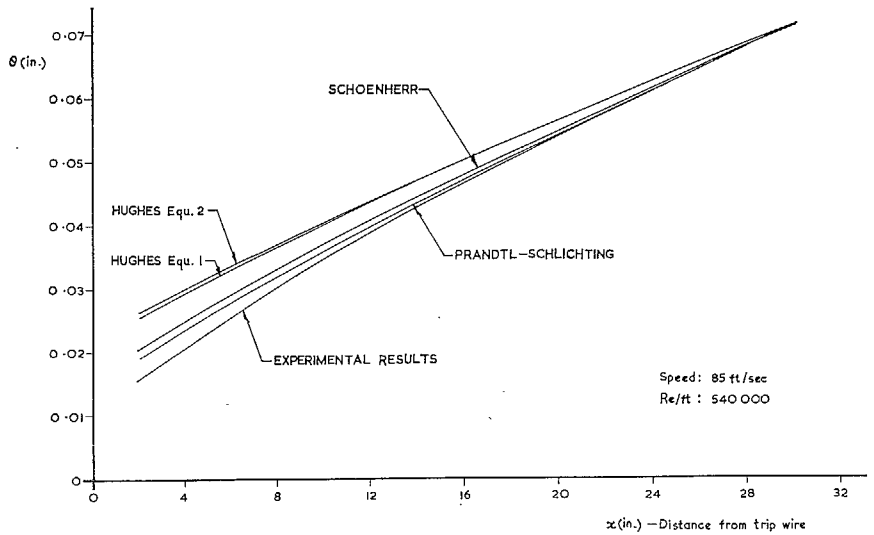

FIG. 6. Comparison of the measured θ growth on the centre-line of the 3D plate with that predicted by four empirical standard laws.

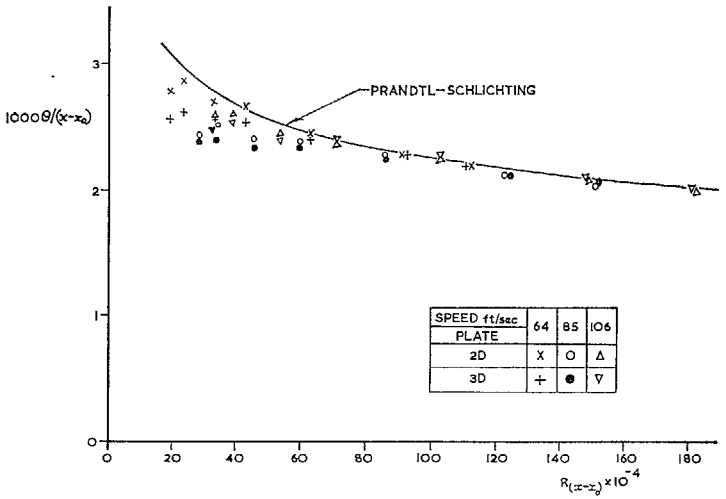

FIG. 7. Experimental variation of $\theta/x = 2C_{F\theta}$.

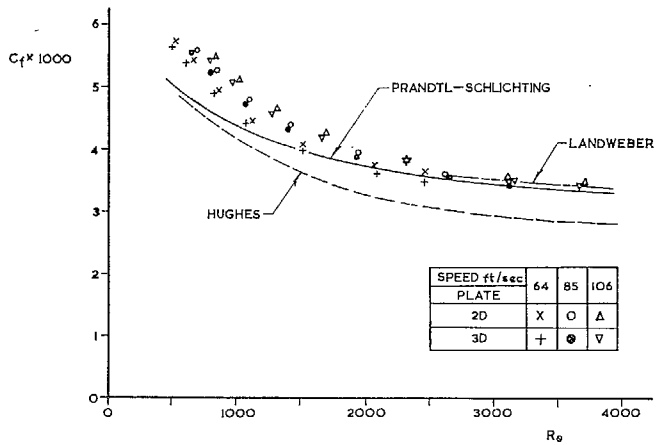

FIG. 8. Experimental variation of C_f.

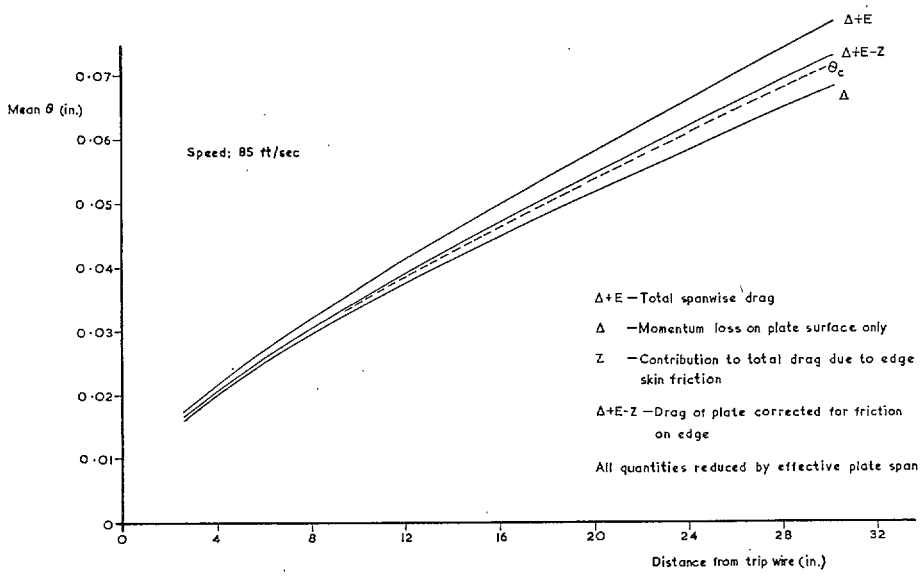

FIG. 9. The components of the total drag of the 3D plate.

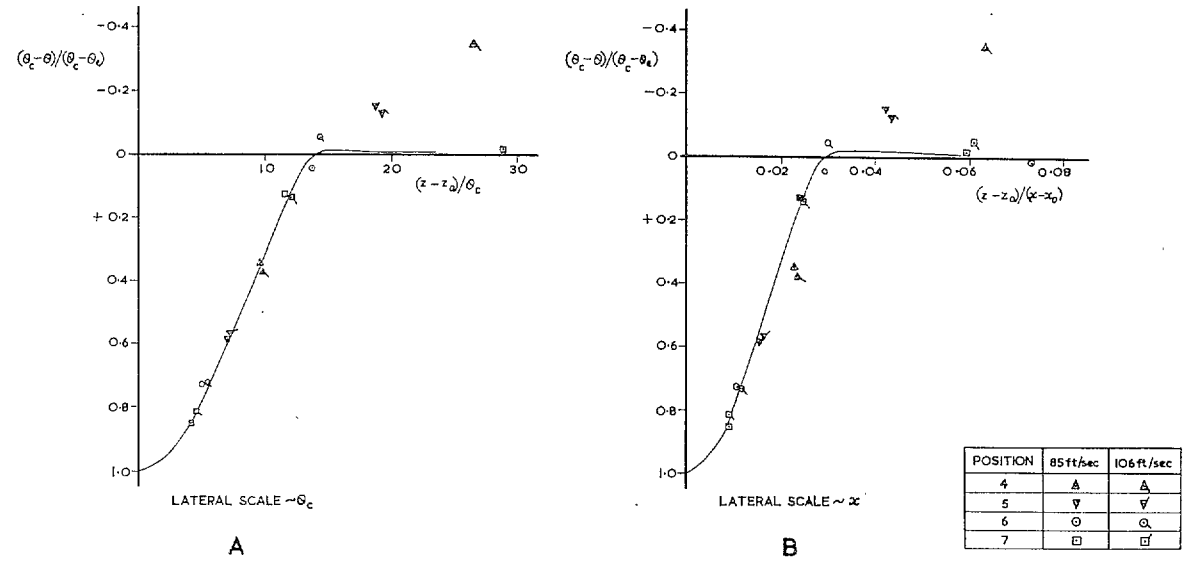

FIG. 10. Reduction of the spanwise distribution of θ near edge in accordance with similarity hypothesis—values plotted are mean of port and starboard distributions.

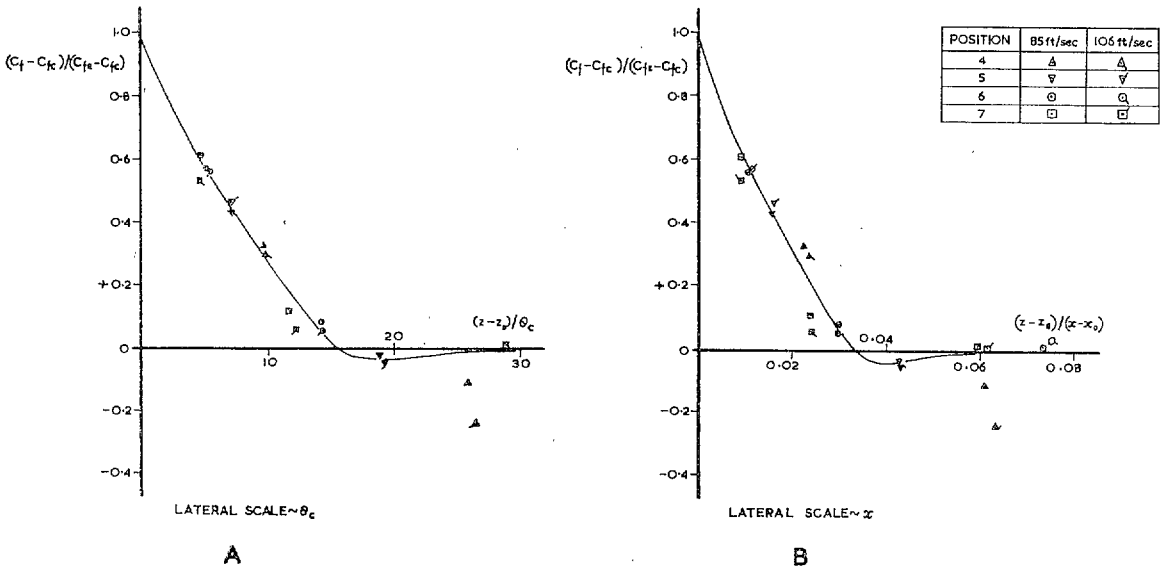

FIG. 11. Reduction of the spanwise distribution of C_f near edge in accordance with similarity hypothesis—values plotted are mean of port and starboard distributions.

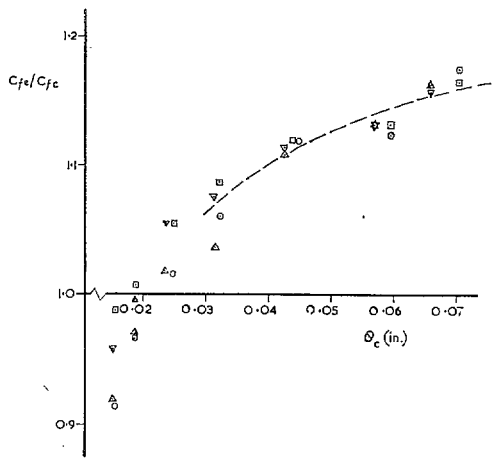

SPEED ft/sec	85	106
Port edge	⊙	△
Starboard edge	⊡	▽

FIG. 12. The development of C_f at the edge of the 3D plate.

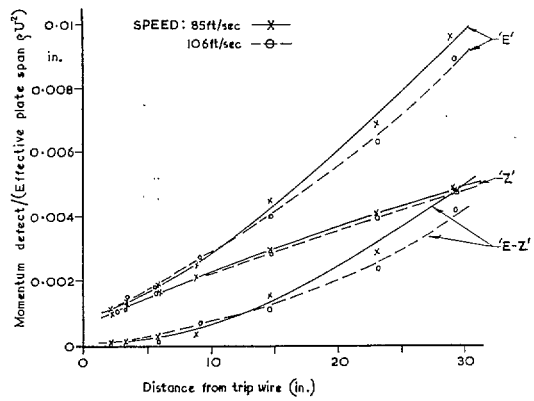

'Z' —Momentum defect due to action of C_{fe} on edge area

'E' —Total momentum defect in region of edge

'E-Z'-Part of E due to edge effect

FIG. 13. The components of the momentum-defect flux off the edge of the 3D plate.

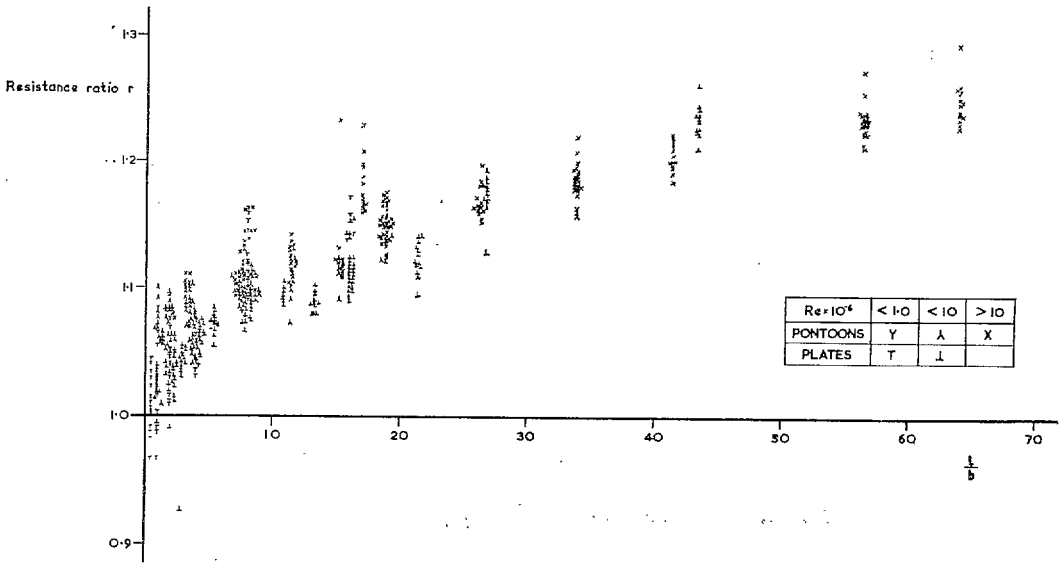

FIG. 14. Hughes' values of the resistance ratio as functions of l/b.

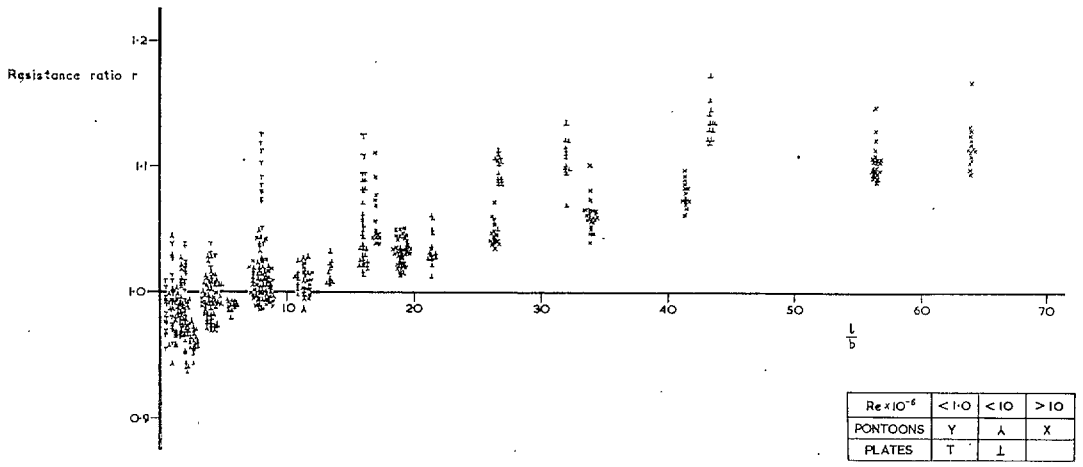

FIG. 15. Data of Fig. 14 replotted using Schoenherr's law for the basic skin friction in two dimensions.

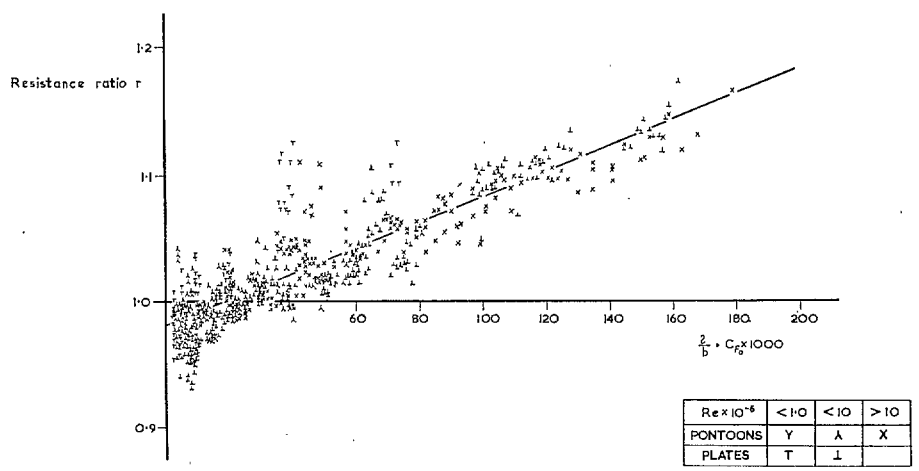

FIG. 16. Replot of Fig. 15 with $(l/b)C_{F0}$ as abscissa.

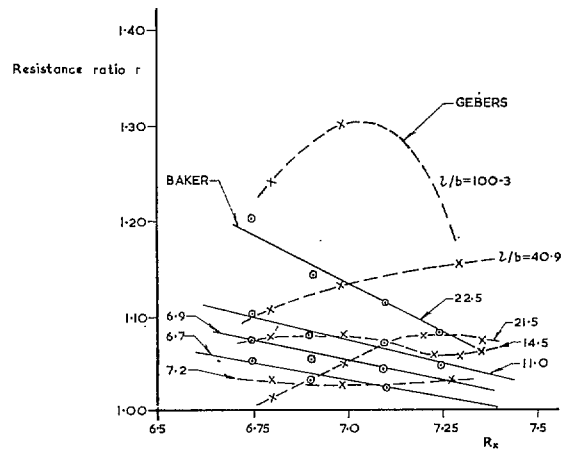

FIG. 17. The effect of edge stimulation of transition on the apparent aspect-ratio effect.

(89338) W . 65/1418 K.5 5/64 Hw.

Publications of the Aeronautical Research Council

ANNUAL TECHNICAL REPORTS OF THE AERONAUTICAL RESEARCH COUNCIL (BOUND VOLUMES)

1942 Vol. I. Aero and Hydrodynamics, Aerofoils, Airscrews, Engines. 75*s.* (post 2*s.* 9*d.*)
Vol. II. Noise, Parachutes, Stability and Control, Structures, Vibration, Wind Tunnels. 47*s.* 6*d.* (post 2*s.* 3*d.*)

1943 Vol. I. Aerodynamics, Aerofoils, Airscrews. 80*s.* (post 2*s.* 6*d.*)
Vol. II. Engines, Flutter, Materials, Parachutes, Performance, Stability and Control, Structures. 90*s.* (post 2*s.* 9*d.*)

1944 Vol. I. Aero and Hydrodynamics, Aerofoils, Aircraft, Airscrews, Controls. 84*s.* (post 3*s.*)
Vol. II. Flutter and Vibration, Materials, Miscellaneous, Navigation, Parachutes, Performance, Plates and Panels, Stability, Structures, Test Equipment, Wind Tunnels. 84*s.* (post 3*s.*)

1945 Vol. I. Aero and Hydrodynamics, Aerofoils. 130*s.* (post 3*s.* 6*d.*)
Vol. II. Aircraft, Airscrews, Controls. 130*s.* (post 3*s.* 6*d.*)
Vol. III. Flutter and Vibration, Instruments, Miscellaneous, Parachutes, Plates and Panels, Propulsion. 130*s.* (post 3*s.* 3*d.*)
Vol. IV. Stability, Structures, Wind Tunnels, Wind Tunnel Technique. 130*s.* (post 3*s.* 3*d.*)

1946 Vol. I. Accidents, Aerodynamics, Aerofoils and Hydrofoils. 168*s.* (post 3*s.* 9*d.*)
Vol. II. Airscrews, Cabin Cooling, Chemical Hazards, Controls, Flames, Flutter, Helicopters, Instruments and Instrumentation, Interference, Jets, Miscellaneous, Parachutes. 168*s.* (post 3*s.* 3*d.*)
Vol. III. Performance, Propulsion, Seaplanes, Stability, Structures, Wind Tunnels. 168*s.* (post 3*s.* 6*d.*)

1947 Vol. I. Aerodynamics, Aerofoils, Aircraft. 168*s.* (post 3*s.* 9*d.*)
Vol. II. Airscrews and Rotors, Controls, Flutter, Materials, Miscellaneous, Parachutes, Propulsion, Seaplanes, Stability, Structures, Take-off and Landing. 168*s.* (post 3*s.* 9*d.*)

1948 Vol. I. Aerodynamics, Aerofoils, Aircraft, Airscrews, Controls, Flutter and Vibration, Helicopters, Instruments, Propulsion, Seaplane, Stability, Structures, Wind Tunnels. 130*s.* (post 3*s.* 3*d.*)
Vol. II. Aerodynamics, Aerofoils, Aircraft, Airscrews, Controls, Flutter and Vibration, Helicopters, Instruments, Propulsion, Seaplane, Stability, Structures, Wind Tunnels. 110*s.* (post 3*s.* 3*d.*)

Special Volumes

Vol. I. Aero and Hydrodynamics, Aerofoils, Controls, Flutter, Kites, Parachutes, Performance, Propulsion, Stability. 126*s.* (post 3*s.*)
Vol. II. Aero and Hydrodynamics, Aerofoils, Airscrews, Controls, Flutter, Materials, Miscellaneous, Parachutes, Propulsion, Stability, Structures. 147*s.* (post 3*s.*)
Vol. III. Aero and Hydrodynamics, Aerofoils, Airscrews, Controls, Flutter, Kites, Miscellaneous, Parachutes, Propulsion, Seaplanes, Stability, Structures, Test Equipment. 189*s.* (post 3*s.* 9*d.*)

Reviews of the Aeronautical Research Council

1939–48 3*s.* (post 6*d.*) 1949–54 5*s.* (post 5*d.*)

Index to all Reports and Memoranda published in the Annual Technical Reports

1909–1947 R. & M. 2600 (out of print)

Indexes to the Reports and Memoranda of the Aeronautical Research Council

Between Nos. 2351–2449	R. & M. No. 2450	2*s.* (post 3*d.*)
Between Nos. 2451–2549	R. & M. No. 2550	2*s.* 6*d.* (post 3*d.*)
Between Nos. 2551–2649	R. & M. No. 2650	2*s.* 6*d.* (post 3*d.*)
Between Nos. 2651–2749	R. & M. No. 2750	2*s.* 6*d.* (post 3*d.*)
Between Nos. 2751–2849	R. & M. No. 2850	2*s.* 6*d.* (post 3*d.*)
Between Nos. 2851–2949	R. & M. No. 2950	3*s.* (post 3*d.*)
Between Nos. 2951–3049	R. & M. No. 3050	3*s.* 6*d.* (post 3*d.*)
Between Nos. 3051–3149	R. & M. No. 3150	3*s.* 6*d.* (post 3*d.*)

HER MAJESTY'S STATIONERY OFFICE

from the addresses overleaf

Printed and published by
HER MAJESTY'S STATIONERY OFFICE

To be purchased from
York House, Kingsway, London W.C.2
423 Oxford Street, London W.1
13A Castle Street, Edinburgh 2
109 St. Mary Street, Cardiff
39 King Street, Manchester 2
50 Fairfax Street, Bristol 1
35 Smallbrook, Ringway, Birmingham 5
80 Chichester Street, Belfast 1
or through any bookseller

Printed in England

S.O. Code No. 23-3367